THE UNIVERSITY OF NEW MEXICO

CQuIC Center for Quantum Information and Control

SAND2020-4714PE

An RF Optically Pumped Magnetometer for Communication through Lossy Media

PRESENTED BY

John Bainbridge

Sandia National Laboratories is a multimission laboratory managed and operated by National Technology & Engineering Solutions of Sandia, LLC, a wholly owned subsidiary of Honeywell International Inc., for the U.S. Department of Energy's National Nuclear Security Administration under contract DE-NA0003525.

Organizational Overview

Part 1: Introduction to our Magnetometer

I. Why quantum sensors for lossy communication?

II. Optically pumped magnetometers(OPM's) for magnetic field sensing in the VLF regime.

Part 2: Theoretical Framework

I. Modeling and the master equation

II. Analysis of optimal species

Part 3: Experimental Results

I. Light narrowing

II. Sensitivity

Part 5: Future Work

Part 4: Acknowledgements

Part 1-I: Why quantum sensors for lossy communication?

Why Atomic Magnetometers?

1. Can achieve sensitivities $\sim 1 \mathrm{f}T/\sqrt{Hz}$, comparable to superconducting quantum interference devices (SQUIDs) without need for cryogenic cooling.[9]
2. Nuclear magnetic resonance (NMR) and nuclear quadrupole resonance(NQR) detection.[3]
3. Fundamental Physics (Axion searches).[1]
4. Radio communication with small signal amplitude.[4]

Lossy Communication and the Skin Effect

In a medium, the strength of an RF signal attenuates due to the skin effect as:

$$A(z) = A_0 e^{-\delta z}.$$

Where $A(z)$ is the amplitude after traveling a distance through z the medium, and:

$$\delta(f) = \sqrt{\frac{1}{\pi \mu_0 \mu_r \sigma f}} \propto 1/\sqrt{f}.$$

Is the *skin depth* of the material, where μ_0 & μ_r are the vacuum and relative permeability of the material, and σ is its conductivity.

→**We cannot effectively communicate through most media at higher frequencies.** But we **can communicate at lower frequencies** with a highly sensitive detector (and sufficiently powerful transmitter!).[4]

The Current State of RF OPM's

- RF OPM's designed for RF field detection have thus far been mostly confined to the laboratory:
  - Initial work was done by the group of M.V. Romalis at Princeton. Focused on fundamental physics, and MRI for medical imaging. [6,7,9,10,12]
  - Leddbetter et al. & Chalupczak et al. demonstrated highly sensitive room temp RF OPM's.[2,5]
  - Savkov, Kim, and Boshier managed to modify a commercial OPM from QuSpin to operate up to 1.7kHz. This frequency range is below what we want to (DC-300kHz). [8]

We aim to create a *fieldable* device that can realize their communication potential.

- Must minimize volume and power requirements
- Must operate outside a shield.

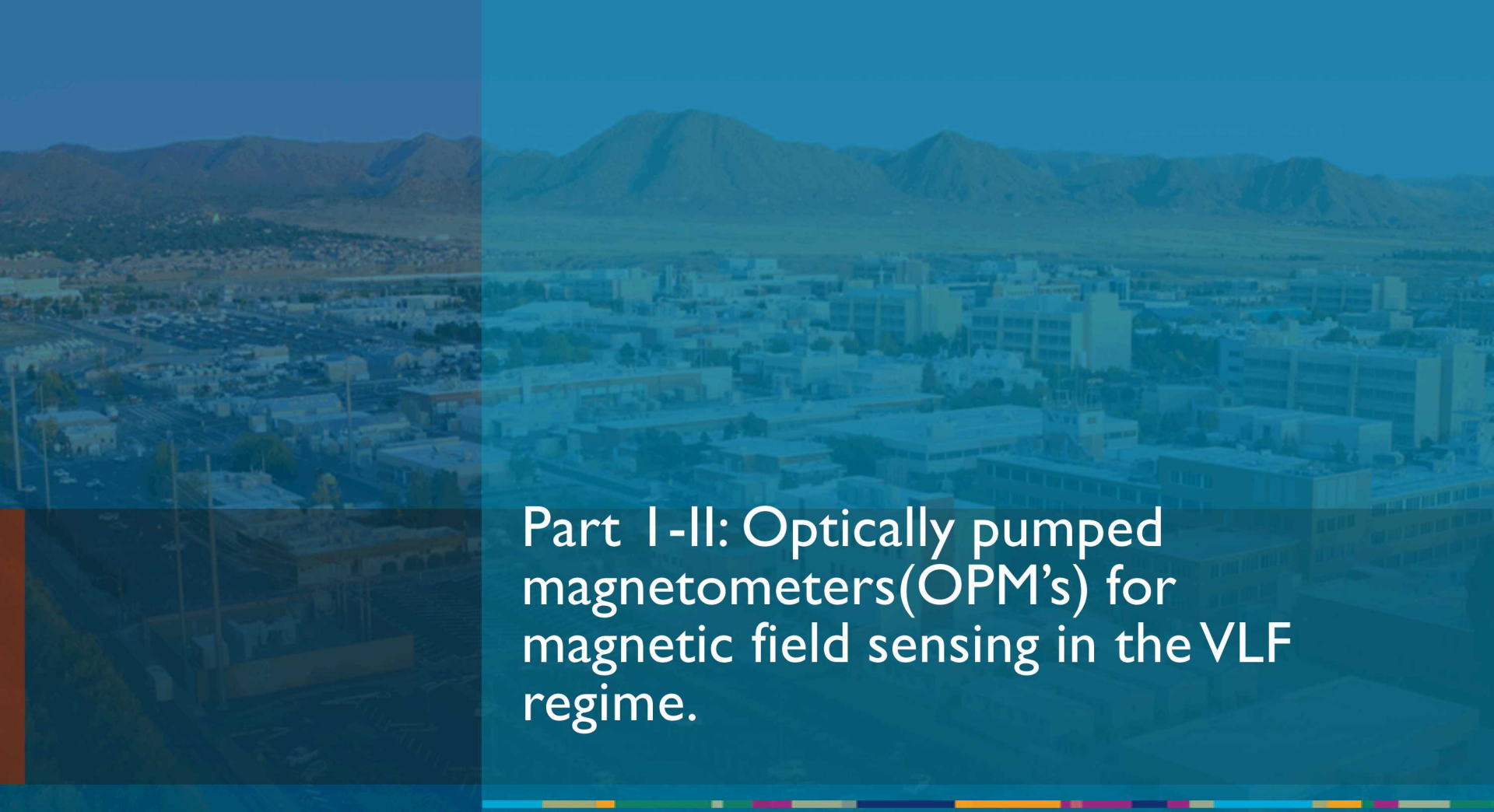

Part 1-II: Optically pumped magnetometers(OPM's) for magnetic field sensing in the VLF regime.

Atomic Magnetometers: Larmor Precession

Exploit the Larmor precession of atoms in a magnetic field $\boldsymbol{B} = \mathrm{B}_0\mathbf{e}_z$

$$\omega_0 = \gamma B_0.$$

Where ω_0 is the Larmor precession frequency and γ is the gyromagnetic ratio.

If we know γ, we can measure ω_0 to measure B_0!

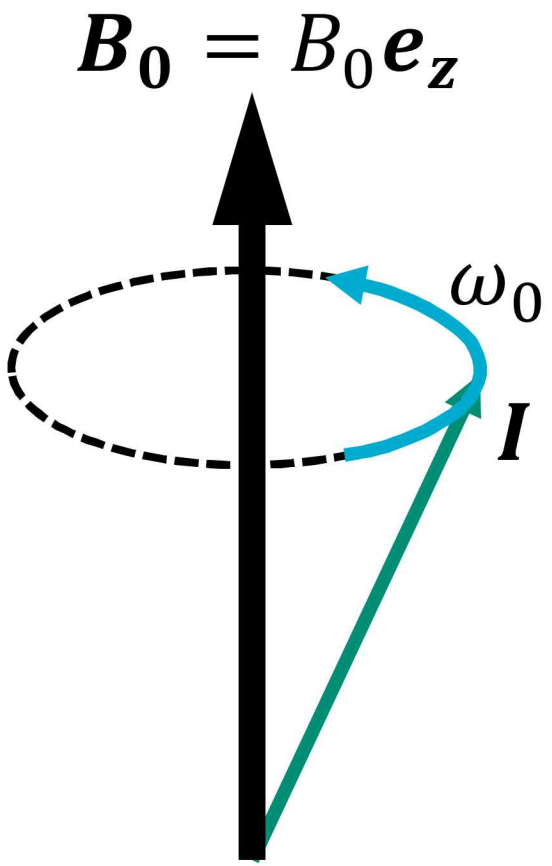

Right: Illustration of Larmor Precession in a static magnetic field

Optically Pumped Magnetometers(OPMs)

Atomic vapor is naturally in the maximally mixed state

$$\rho = \frac{1}{N}\mathbb{I}_N.$$

Where the Hilbert space of the atom has N total states and $\mathbb{I}_N$ is the $N \times N$ identity operator.

Before measuring precession, the state must be optically pumped into a metrologically useful state such as the "stretched state":

$$\rho = |F_a, m_F = F_a\rangle\langle F_a, m_F = F_a|.$$

Where $F_a = I + 1/2$ and

$F_b = I - 1/2$.

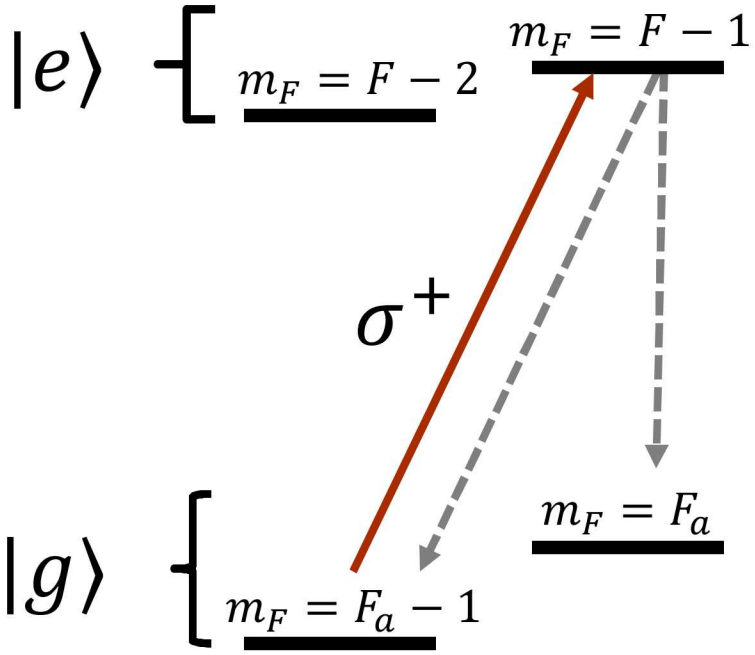

Above: Optical pumping with σ^+ polarized light causes population to accumulate in the "stretched" sate.

RF Magnetometry

Consider the effect an RF field transverse to $\boldsymbol{B_0}$:

$$\boldsymbol{B_{RF}}(t) = B_{RF}\sin(\omega_{RF}t)\,\boldsymbol{e_x}$$

Causes the state to rotate around $\boldsymbol{e_z}$ at frequency ω_{RF} and oscillate between $\pm\,\boldsymbol{e_z}$ at frequency

$$\Omega' = \sqrt{(\Delta\omega)^2 + \Omega^2}.$$

Where $\Delta\omega = \omega_{RF} - \omega_0$ and

$$\Omega = \frac{1}{2}\gamma B_{RF}.$$

Factor of $\frac{1}{2}$ because half the RF field is corotating. Other half is counterrotating, and can be neglected in RWA.

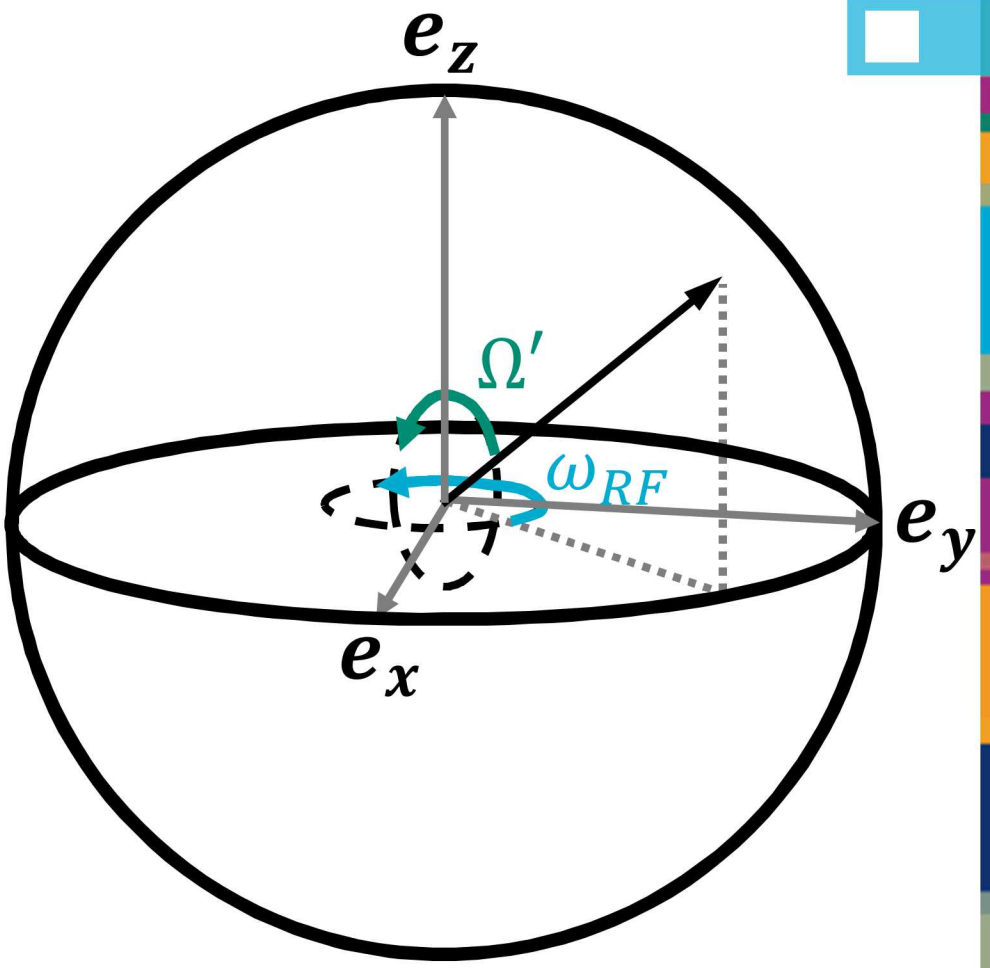

Above: Bloch sphere picture of the dynamics of the state in an RF magnetic field.

Practical RF Magnetometry

1. Pick frequency to measure f.
2. Tune B_0 so $f = \omega_0/2\pi$.
3. With $\omega_0 \approx \omega_{RF}$, measure $\langle S_x(t)\rangle = \gamma B_{RF}[\alpha \cos(\omega_{RF} t) + \beta \sin(\omega_{RF} t)]$.

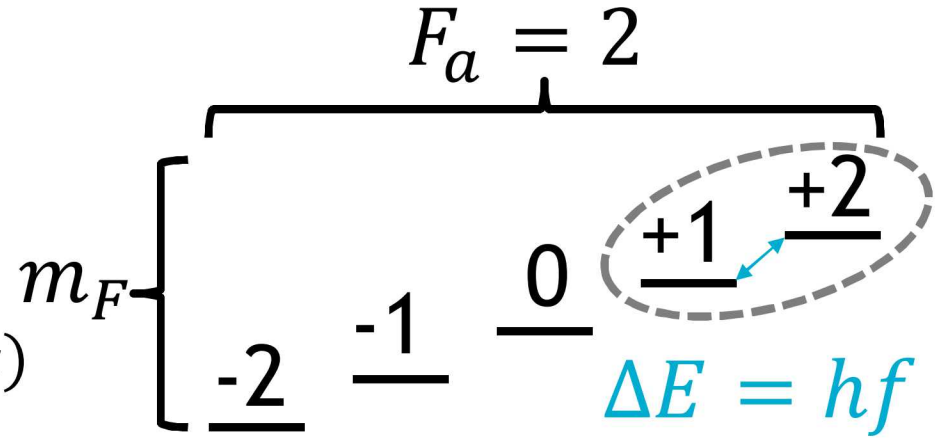

Right: Hyperfine ground state manifold of an $I = \frac{3}{2}$ alkali atom such as ^{87}Rb, with the Zeeman resonance of interest marked.

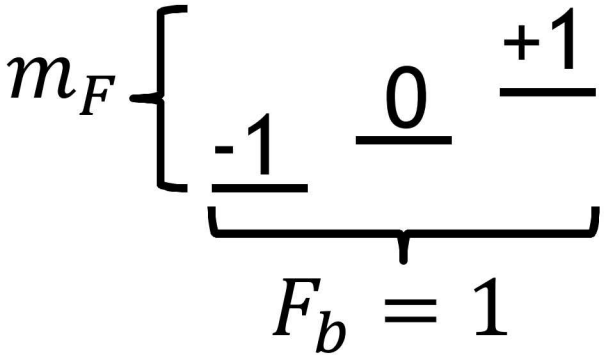

The Experimental Layout

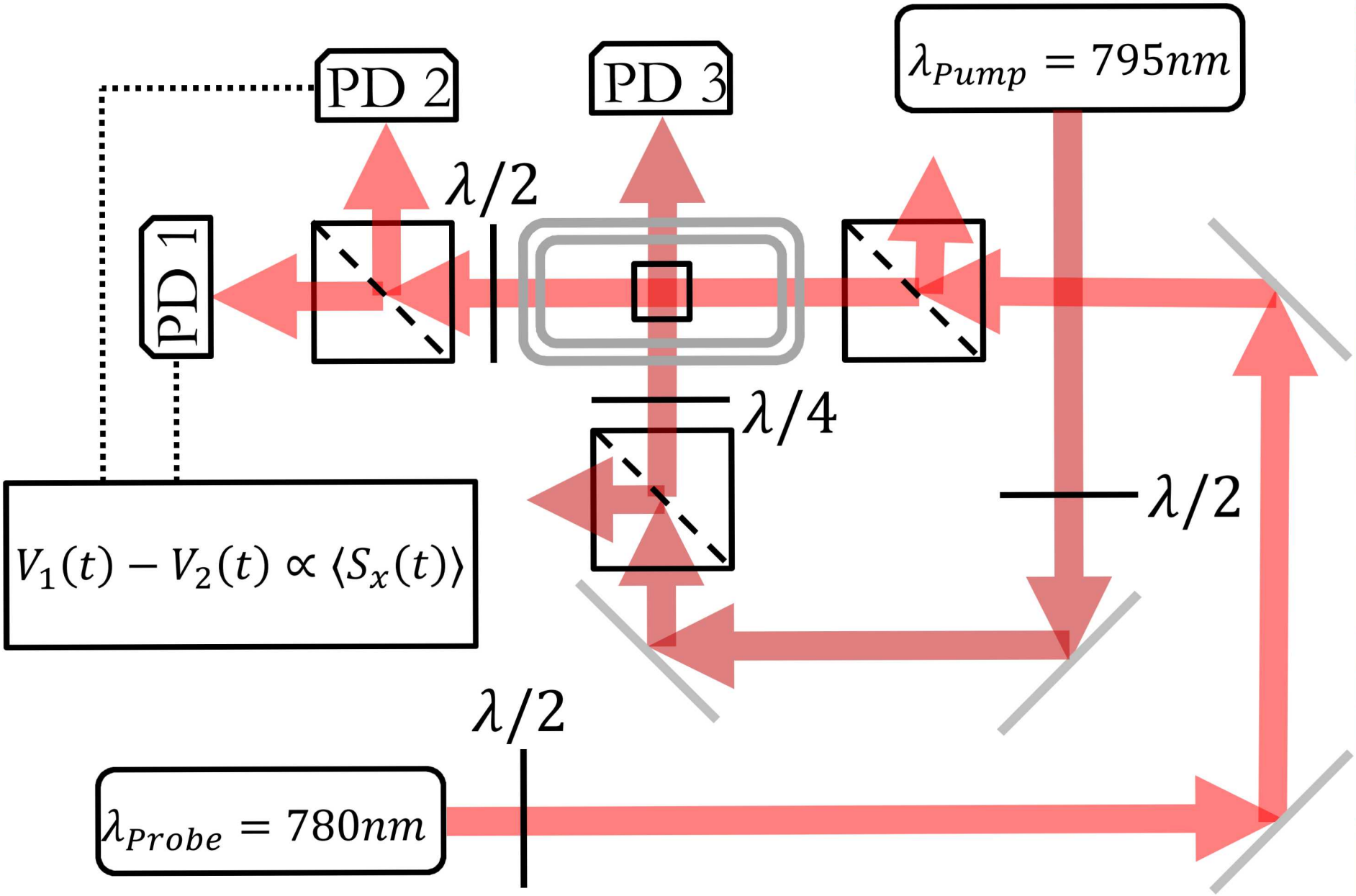

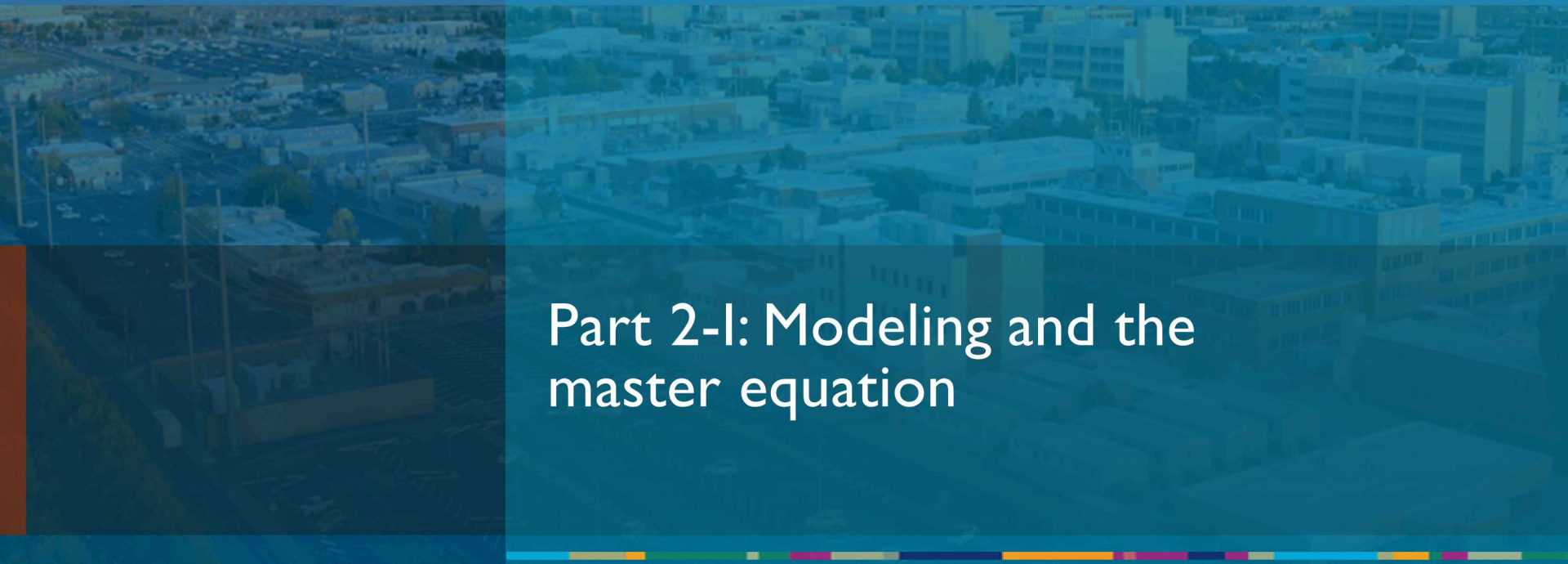

Part 2-I: Modeling and the master equation

The Master Equation

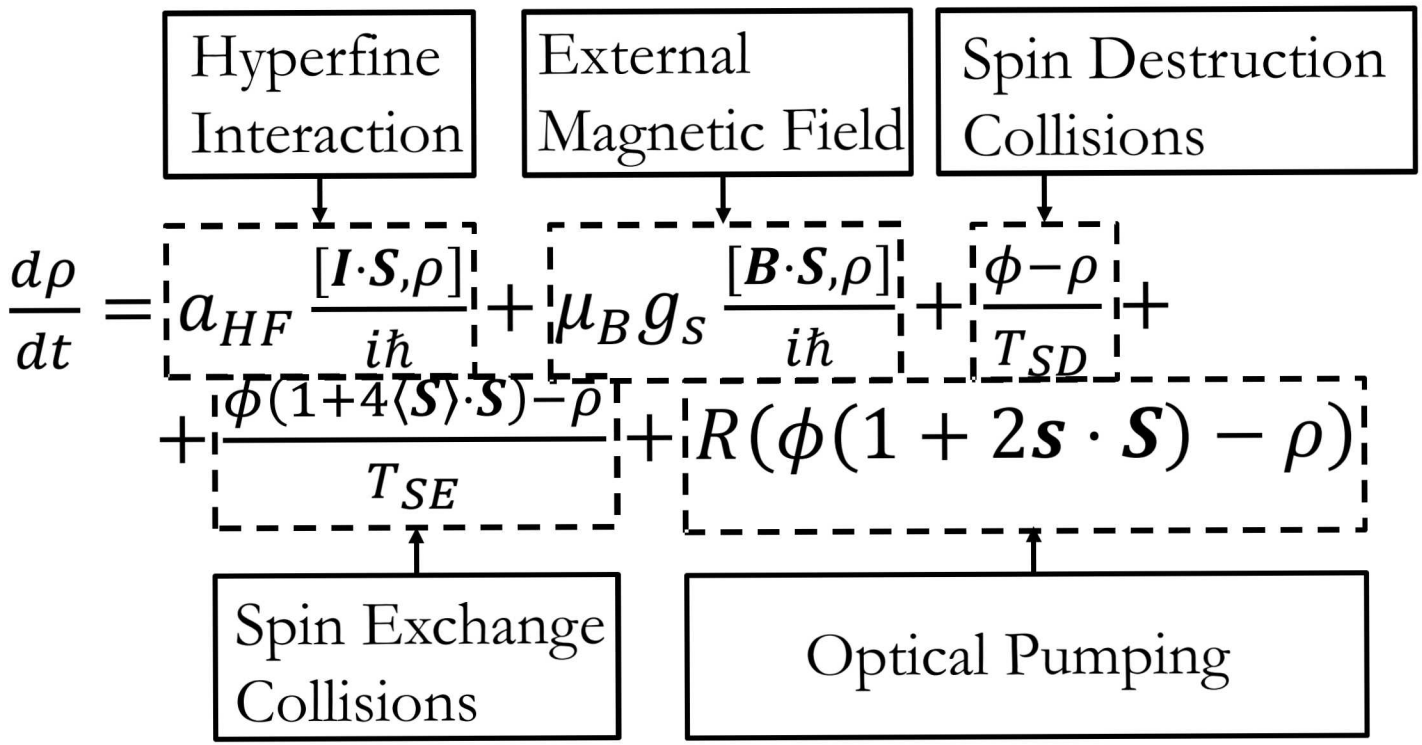

The Hyperfine Interaction

$$\left(\frac{d\rho}{dt}\right)_{Hyperfine} = a_{HF}[\boldsymbol{I}\cdot\boldsymbol{S},\rho]$$

This is the term from the free evolution of a single atom in vacuum.

- a_{HF} is the hyperfine coupling constant. It can be found in the literature.
- $\boldsymbol{I}$ is an $(N\times N)\times 3$ vector operator representing the nuclear spin of an atom.
- $\mathbf{S}$ is an $(N\times N)\times 3$ vector operator representing the electron spin of an atom.

Magnetic Field Coupling

$$\left(\frac{d\rho}{dt}\right)_{Mag} = \mu_B g_s \frac{[\boldsymbol{B}\cdot\boldsymbol{S},\rho]}{i\hbar}$$

- $\mu_B = 9.2740100783(28)\times 10^{-24}\frac{J^*}{T}$ is the Bohr Magneton.
- $g_s = 2.00231930436256(35)^*$ is the electron g-factor.
- $\hbar = \frac{1}{2\pi}6.62607015\times 10^{-34} J\cdot S^*$ is the reduced Plank's constant.
- $\boldsymbol{B} = B\boldsymbol{e_n}$ where B is a scalar in Teslas, and $\boldsymbol{e_n}$ is a 1×3 vector of unit length.

This term represents the interaction of the electron spin with an external magnetic field. The nuclear spin coupling is ~ 1000 times smaller, and can be neglected.

*CODATA values from NIST.

Spin Destroying Collisions

$$\left(\frac{d\rho}{dt}\right)_{SD} = \frac{\phi - \rho}{T_{SD}}$$

- $\phi = \rho/4 + \boldsymbol{S} \cdot \rho \boldsymbol{S}$ is the part of the density operator with only nuclear spin polarization $\Rightarrow \rho - \phi$ is the part with electron spin polarization.
- $R_{SD} = \frac{1}{T_{SD}} = \sum_j n_j \bar{v}_j \sigma_{SD,j}$ is the total spin destruction rate.
  - n_j is the density of the jth species with which the atoms are interacting
  - $\bar{v}_j$ is the average center of mass speed of the atoms relative to those of the jth species.
  - $\sigma_{SD,j}$ is the interaction cross section for spin−depolarizing collisions with the jth species.

This term represents the loss of coherence due to collisions that destroy the electron spin polarization.

Spin Exchanging Collisions

$$\left(\frac{d\rho}{dt}\right)_{SE} = \frac{\phi(1 + 4\langle \boldsymbol{S} \rangle \cdot \boldsymbol{S}) - \rho}{T_{SE}}$$

- $\frac{\phi - \rho}{T_{SE}}$ represents loss of coherence due to the collisions that exchange the spin between particles ($\boldsymbol{S}_1 \rightarrow \boldsymbol{S}_2$ & $\boldsymbol{S}_2 \rightarrow \boldsymbol{S}_1$).
- $\frac{4\phi\langle \boldsymbol{S} \rangle \cdot \boldsymbol{S}}{T_{SE}}$ gives the rate of redistribution of spin polarization from the spin exchange collisions, as the average spin $\langle \boldsymbol{S} \rangle = Tr(\rho \boldsymbol{S})$ of the ensemble interacts with spin of the individual electrons $\boldsymbol{S}$.
- $R_{SE} = \frac{1}{T_{SE}} = n\bar{v}\sigma_{SE}$ is the rate of spin exchange collisions, where n is the density, $\bar{v}$ is the average relative center of mass speed, and σ_{SE} is the interaction cross section for spin-exchanging collisions.

This complicated term describes how spin-exchanging collisions between alkali atoms both causes decoherence and redistributes spin polarization throughout the hyperfine manifold.

Optical Pumping

$$\left(\frac{d\rho}{dt}\right)_{OP} = R(\phi(1 + 2\boldsymbol{s}\cdot\boldsymbol{S}) - \rho)$$

- $R(\phi - \rho)$ represents loss of coherence due to the optical pumping field.
- $2R\phi\boldsymbol{s}\cdot\boldsymbol{S}$ represents the interaction of the average spin $\boldsymbol{s} = s\boldsymbol{e_n}$ of the photons in the pumping field with the spin $\boldsymbol{S}$ of the electron(s).

This term represents the interaction of the atom(s) with the light field used for optical pumping.

Setting up the Calculation

- All operators can be represented as $N \times N$ matrices, where $N = 2(2I + 1)$.
- Angular momentum operators $\boldsymbol{F}, \boldsymbol{I}, \boldsymbol{S}$ can be found in spherical basis.
  - $\boldsymbol{e}_{\pm 1} = \mp \frac{1}{\sqrt{2}} \boldsymbol{e}_{\boldsymbol{x}} - \frac{i}{\sqrt{2}} \boldsymbol{e}_{\boldsymbol{y}}$, $\boldsymbol{e}_{\boldsymbol{0}} = \boldsymbol{e}_{\boldsymbol{z}}$
  - Find $\langle F, m_F | \boldsymbol{J} | F', m_{F'} \rangle$ for convenient values of F, m_F using ladder operators, where $\boldsymbol{J} = \boldsymbol{F}, \boldsymbol{S}$.
  - From Wigner-Eckart theorem:

$$\langle F, m_F \left| \boldsymbol{J}_q \right| F', m_{F'} \rangle = \langle F', m_{F'}, 1, q | F, m_F \rangle \langle F \left|\left| \boldsymbol{J} \right|\right| F' \rangle.$$

Where $q = \pm 1, 0$ is the spherical index. The first term on the right is a Clebsch-Gordan coefficient, and the second is a reduced matrix element.

- With operators in hand, calculate $\frac{d\rho}{dt}$ for a given input state ρ

MATLAB Implementation: The Basis Representation

The basis is illustrated below for $I = \frac{3}{2}$. m_F values are in ascending order, so $\rho_{11} = |F_b, m_F = -F_b\rangle\langle F_b, m_F = -F_b|$, $\rho_{22} = |F_b, m_F = -F_b + 1\rangle\langle F_b, m_F = -F_b + 1|$ etc. After the lower hyperfine manifold, it restarts at the bottom of the upper manifold, so $\rho_{44} = |F_a, m_F = -F_a\rangle\langle F_a, m_F = -F_a|$, etc.

$F = F_b = 1$

$$\rho = \begin{matrix} \rho_{11} & \rho_{12} & \rho_{13} \\ \rho_{21} & \rho_{22} & \rho_{23} \\ \rho_{31} & \rho_{32} & \rho_{33} \\ \rho_{41} & \rho_{42} & \rho_{43} \\ \rho_{51} & \rho_{52} & \rho_{53} \\ \rho_{61} & \rho_{62} & \rho_{63} \\ \rho_{71} & \rho_{72} & \rho_{73} \\ \rho_{81} & \rho_{82} & \rho_{83} \end{matrix} \begin{matrix} \rho_{14} & \rho_{15} & \rho_{16} & \rho_{17} & \rho_{18} \\ \rho_{24} & \rho_{25} & \rho_{26} & \rho_{27} & \rho_{28} \\ \rho_{34} & \rho_{35} & \rho_{36} & \rho_{37} & \rho_{38} \\ \rho_{44} & \rho_{45} & \rho_{46} & \rho_{47} & \rho_{48} \\ \rho_{54} & \rho_{55} & \rho_{56} & \rho_{57} & \rho_{58} \\ \rho_{64} & \rho_{65} & \rho_{66} & \rho_{67} & \rho_{68} \\ \rho_{74} & \rho_{75} & \rho_{76} & \rho_{77} & \rho_{78} \\ \rho_{84} & \rho_{85} & \rho_{86} & \rho_{87} & \rho_{88} \end{matrix}$$

$F = F_a = 2$

MATLAB Implementation: Simulation Procedure

1. A set of functions calculates $a_{HF}, 1/T_{SE}, 1/T_{SD}$ at a given temperature from literature values for given species.
2. Another function calculates $\boldsymbol{F}, \boldsymbol{I}, \boldsymbol{S}$ from the value of I for the alkali in question.
3. A third function takes these along with an input state ρ, an external magnetic field $\boldsymbol{B}$, and the mean photon polarization vector $\boldsymbol{s}$ to compute the evolution $\frac{d\rho}{dt}$.
4. An initial state ρ_0, mean photon polarization $\boldsymbol{s}$, and magnetic field $\boldsymbol{B}$(t) are chosen and used with the evolution function to feed into built in ODE solver.
   - Solutions are "stiff", requiring use of correct ODE solver.
5. Out comes $\rho(t)$!

We will use this method to compare to experiment in section 3-I.

Part 2-II: Analysis of Optimal Species

The Fundamental Sensitivity

There are three types of quantum fluctuation that ultimately limit the fundamental sensitivity. They are:

1. The spin projection noise: δB_{spn}.
2. The photon shot noise: δB_{psn}.
3. The light shift noise: δB_{lsn}.

The overall noise floor is given by their quadrature sum:

$$\delta B = \sqrt{\delta B_{spn}^2 + \delta B_{psn}^2 + \delta B_{lsn}^2}. \quad (12)$$

Among these, the photon shot noise usually dominates.

Our challenge is to reduce the technical noise (magnetic field noise, current noise, thermal noise, etc.) to this limit.

A Useful Approximation to the Fundamental Sensitivity

For our experimental conditions, a good approximation is:

$$\delta B = \frac{1}{\gamma\sqrt{nV}}\sqrt{\frac{4}{T_2} + \frac{R_{pr}OD}{32} + \frac{8}{R_{pr}ODT_2^2\eta}}. \quad (10)$$

- $\gamma = \gamma_e/(2I+1)$ is the gyromagnetic ratio of the isotope with nuclear spin I, where γ_e is the gyromagnetic ratio of a bare electron.
- n is the density of alkali metal in the vapor cell.
- V is the overlap volume of the pump and probe laser(s).
- T_2 is the transverse spin relaxation time (inverse of bandwidth).
- R_{pr} is the optical pumping rate of the probe beam.
- $OD = \sigma_0 nl$ is the optical depth of the vapor cell.
- η is the quantum efficiency of the detector.

The Best Achievable Sensitivity

One can minimize the RF linewidth and corresponding probe pumping rate to get the best possible sensitivity:

- $\Gamma_{RF}^{Min} = \frac{1}{T_2^{Max}} = \sqrt{\frac{4GR_{SE}R_{SD}}{2I+1}}$
  - $G \approx (1/5, 3/10, 5/14)$ for $I = (3/2, 5/2, 7/2)$.[12]
- $R_{pr}^{Min} OD = \frac{4(2I+1)\Gamma_{RF}^{Min}}{\eta}$.

I optimistically took $\eta = 1$ and $V = 1cm^3$ for these results. The alkali density was computed from the formula from the 1995 edition of the CRC Handbook for saturated vapor pressure at a given temperature.

Results in Potassium

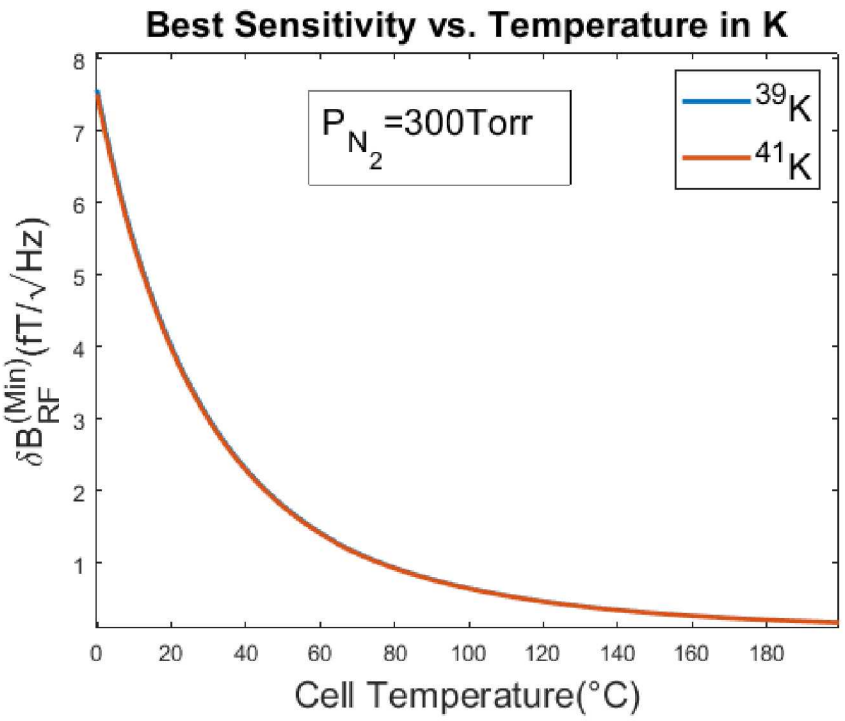

Above Left: The best achievable sensitivity in potassium vs. temperature. The two species overlap almost completely

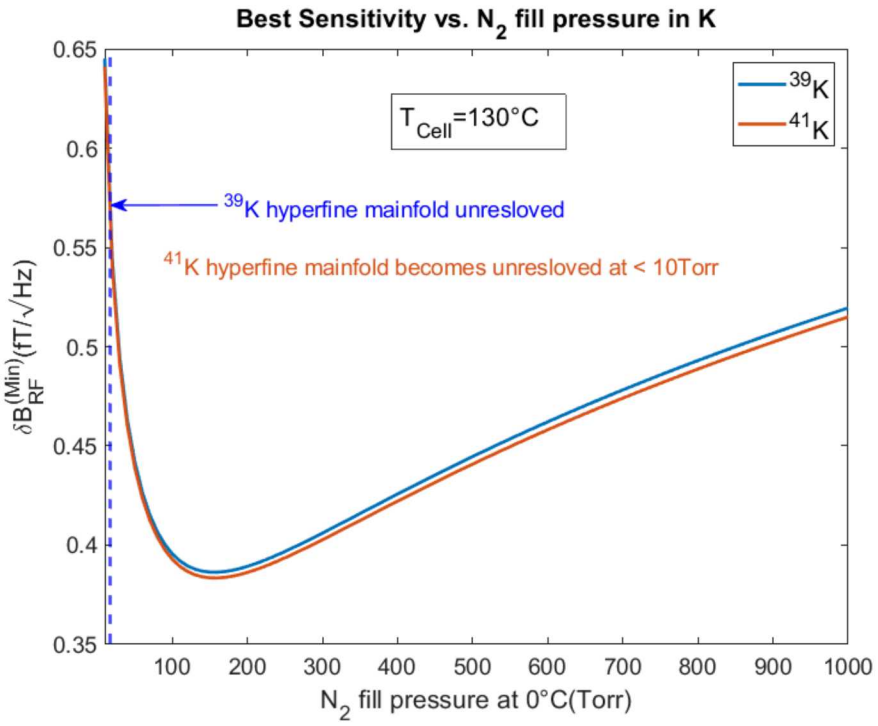

Above Right: The best achievable sensitivity in potassium vs. buffer gas pressure.

Results in Rubidium

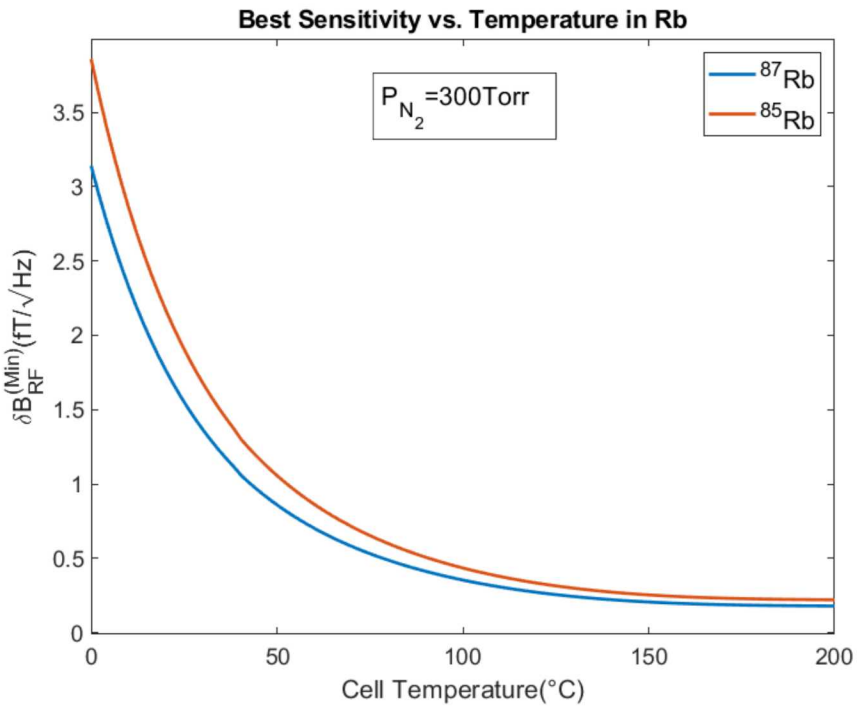

Above left: The best achievable sensitivity in rubidium as a function of temperature.

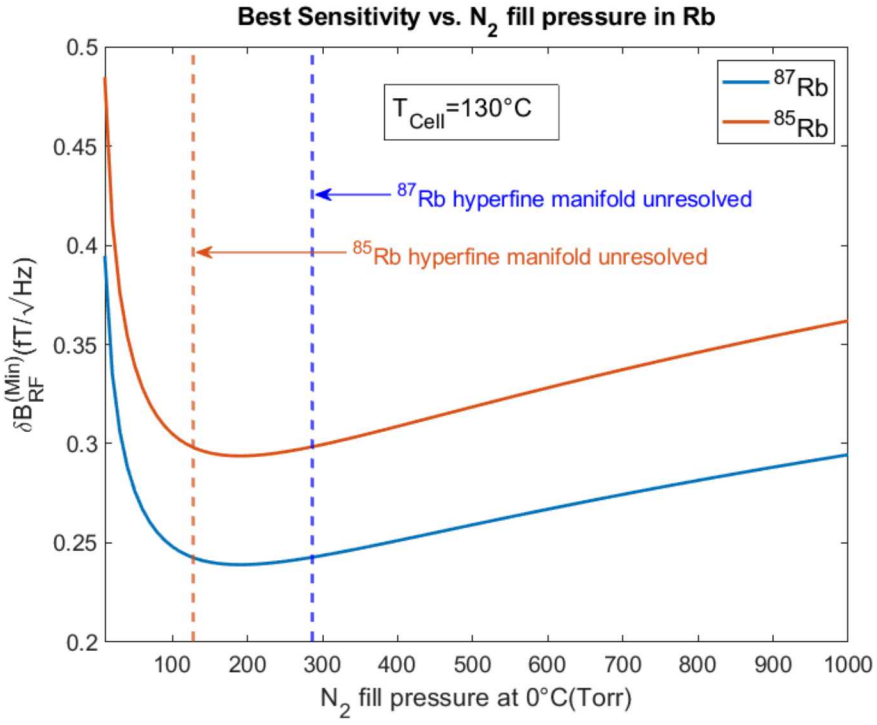

Above Right: The best achievable sensitivity in rubidium vs. buffer gas pressure.

Results in Cesium

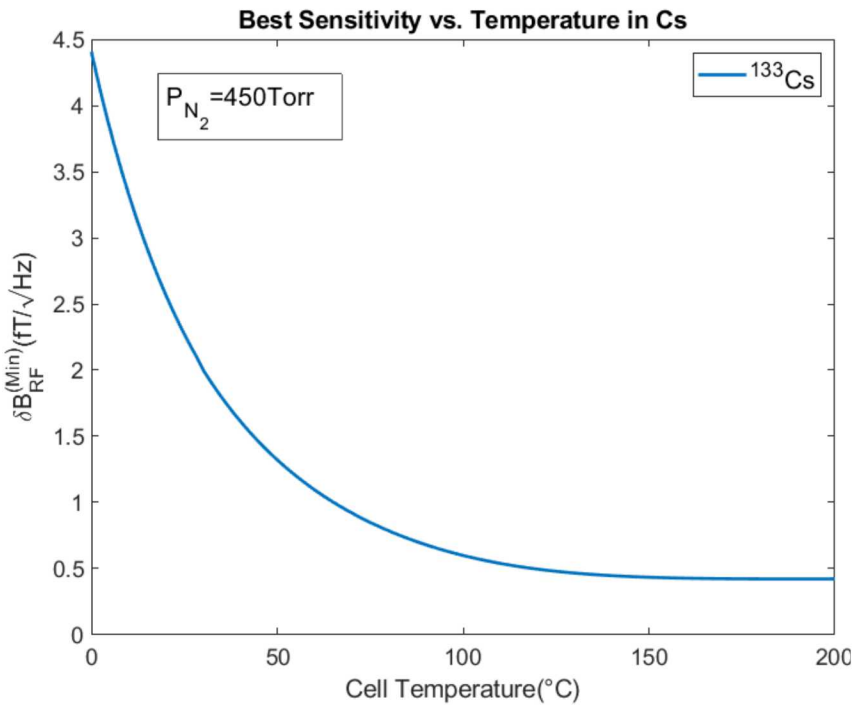

Above Left: The best achievable sensitivity in cesium vs. temperature.

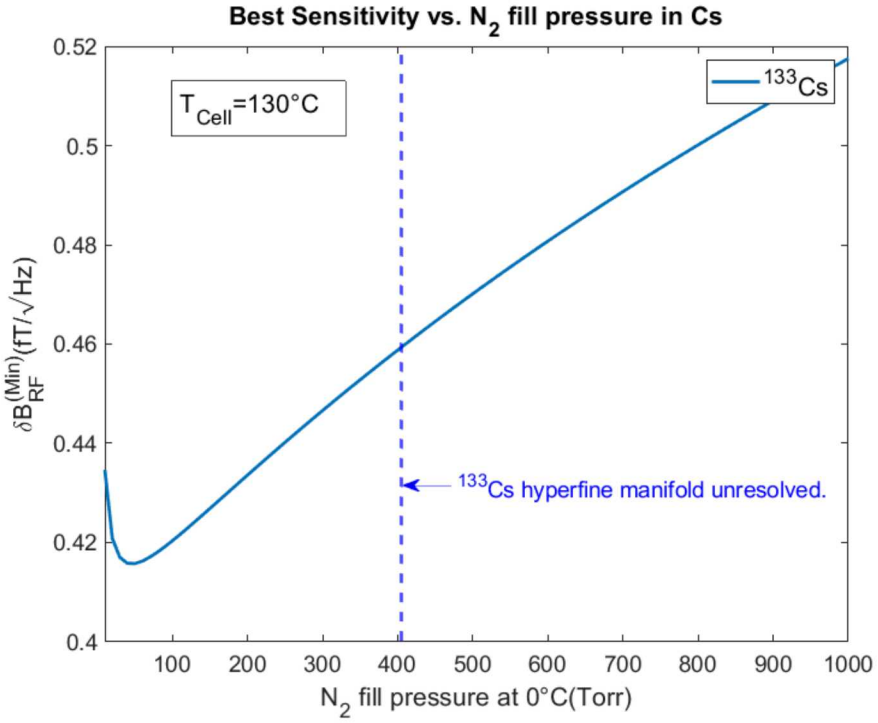

Above Right: The best achievable sensitivity in cesium vs. buffer gas fill pressure.

Conclusions on Species

1. Can achieve a good sensitivity of $< 10\mathrm{fT}/\sqrt{Hz}$ using *any* alkali species.
2. There is relatively little difference between different isotopes of the same species. Isotopically enriched vapor should be used to prevent line broadening due to spin exchange between isotopes.
3. Best option appears to be rubidium. Cesium has a higher limit for marginal improvement at lower temperature. Potassium requires too much heating.
4. Buffer gas pressure should be just enough to prevent hyperfine resolution.

Part 3-I: Light Narrowing.

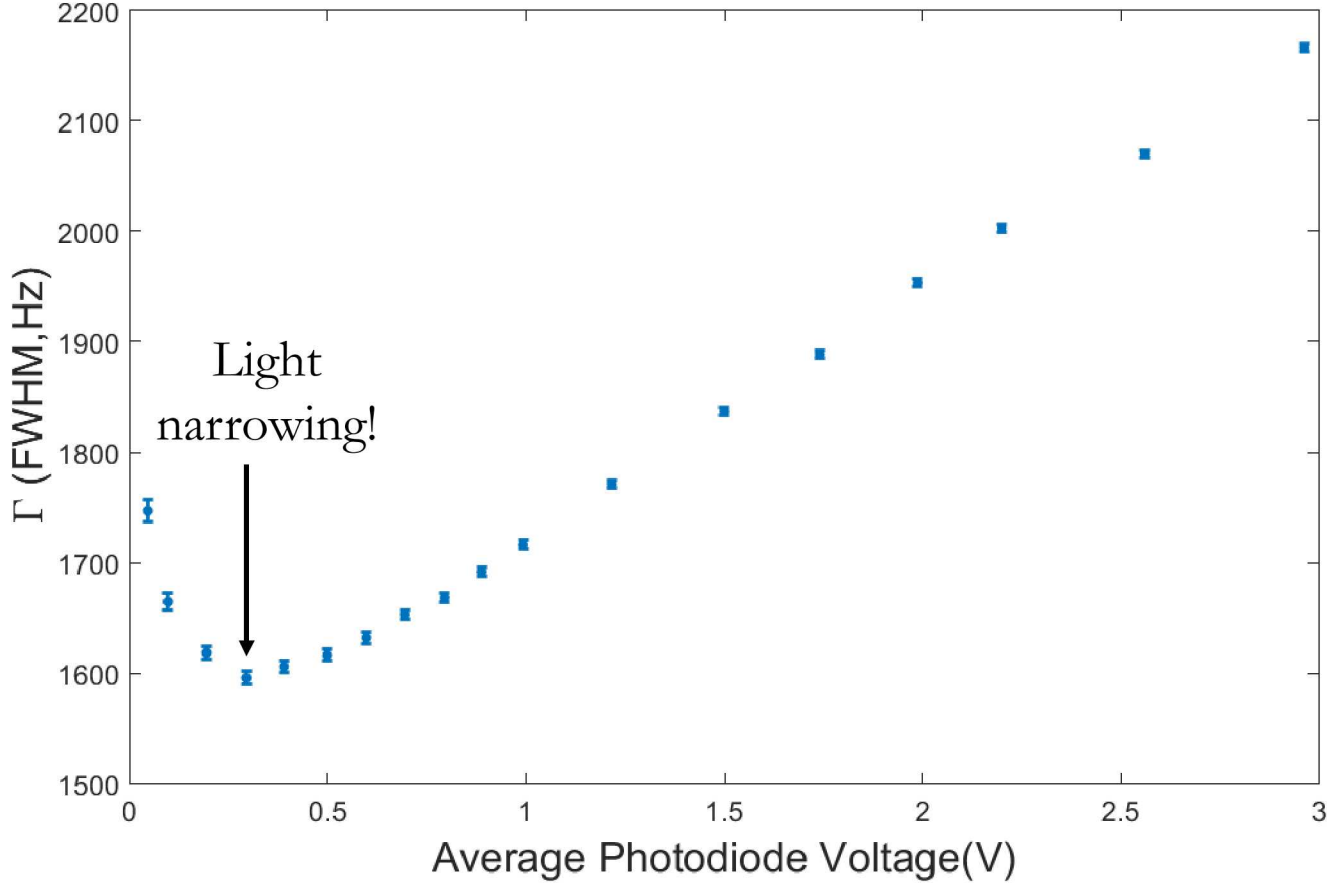

Above: Data showing the dependence of the Zeeman resonance linewidth Γ on the power of the optical pumping beam. Error bars are 95% confidence bounds of Lorentzian fit. The resonance frequency was $f_0 = 2\pi\omega_0 \approx 24.125kHz$ for these measurements.

Extraction of the Pumping Rate

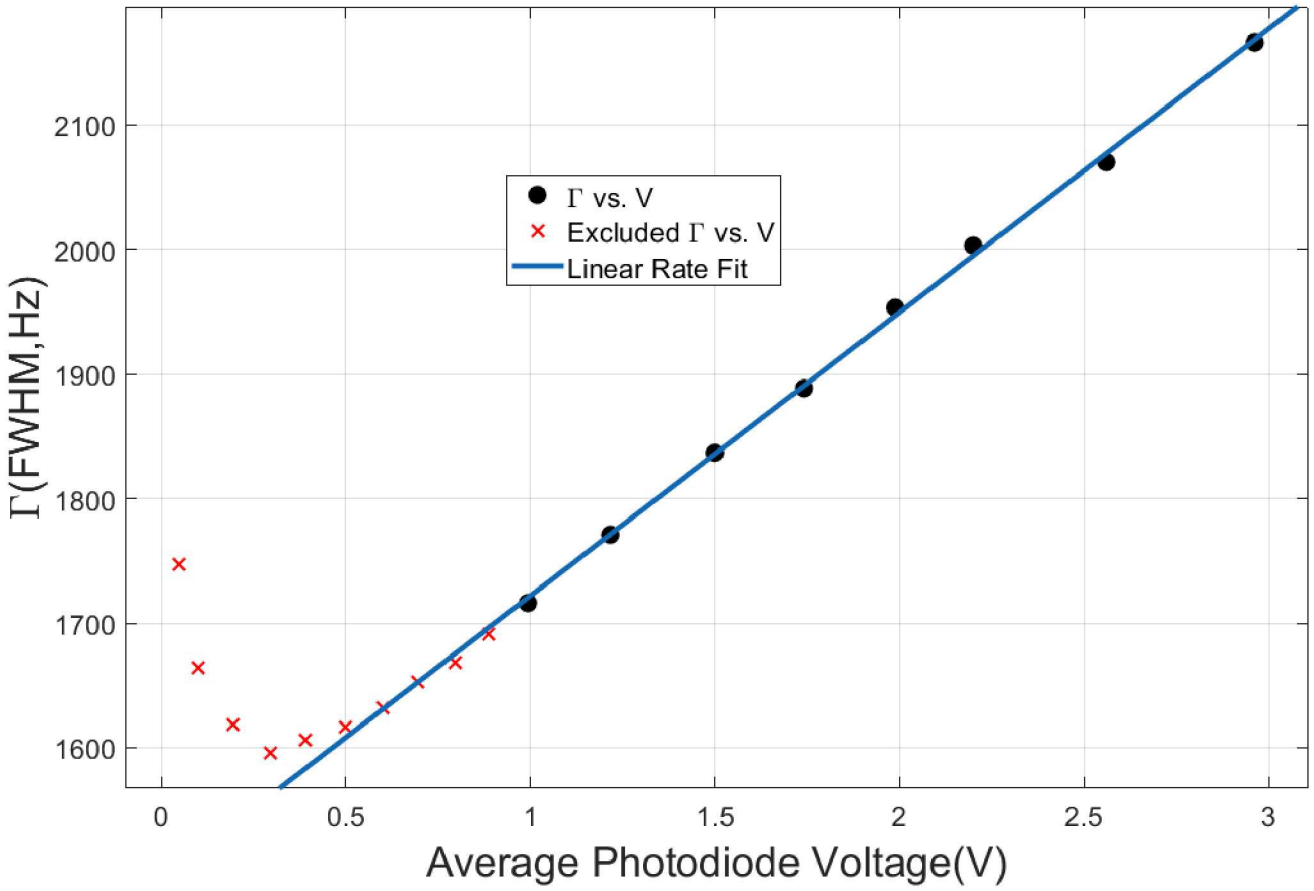

Above: Linear fit to the equation $\Gamma \approx \frac{R_{OP}}{4}$+b for $\frac{R_{SD}R_{SE}}{R_{OP}^2} \ll 1$.[10] A fit to $\Gamma = \frac{aV}{4} + \mathrm{b}$ thus gives $R_{OP} = aV$. This fit gives $a = 910.2(879.5,940.8)s^{-1}/V$.

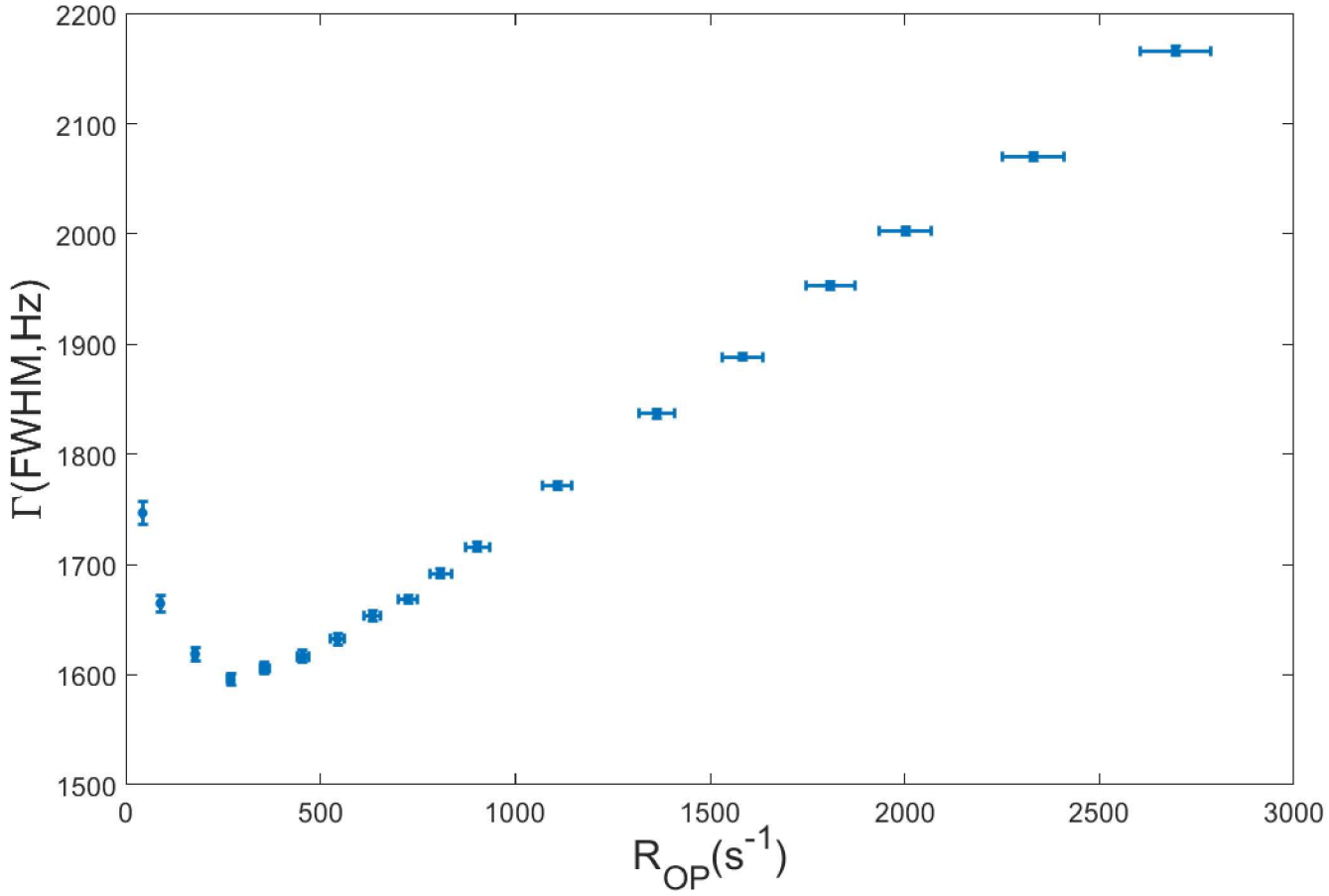

Above: The linewidth as a function of optical pumping rate with error bars given by 95% confidence intervals of the linear fit.

Comparison with Theory

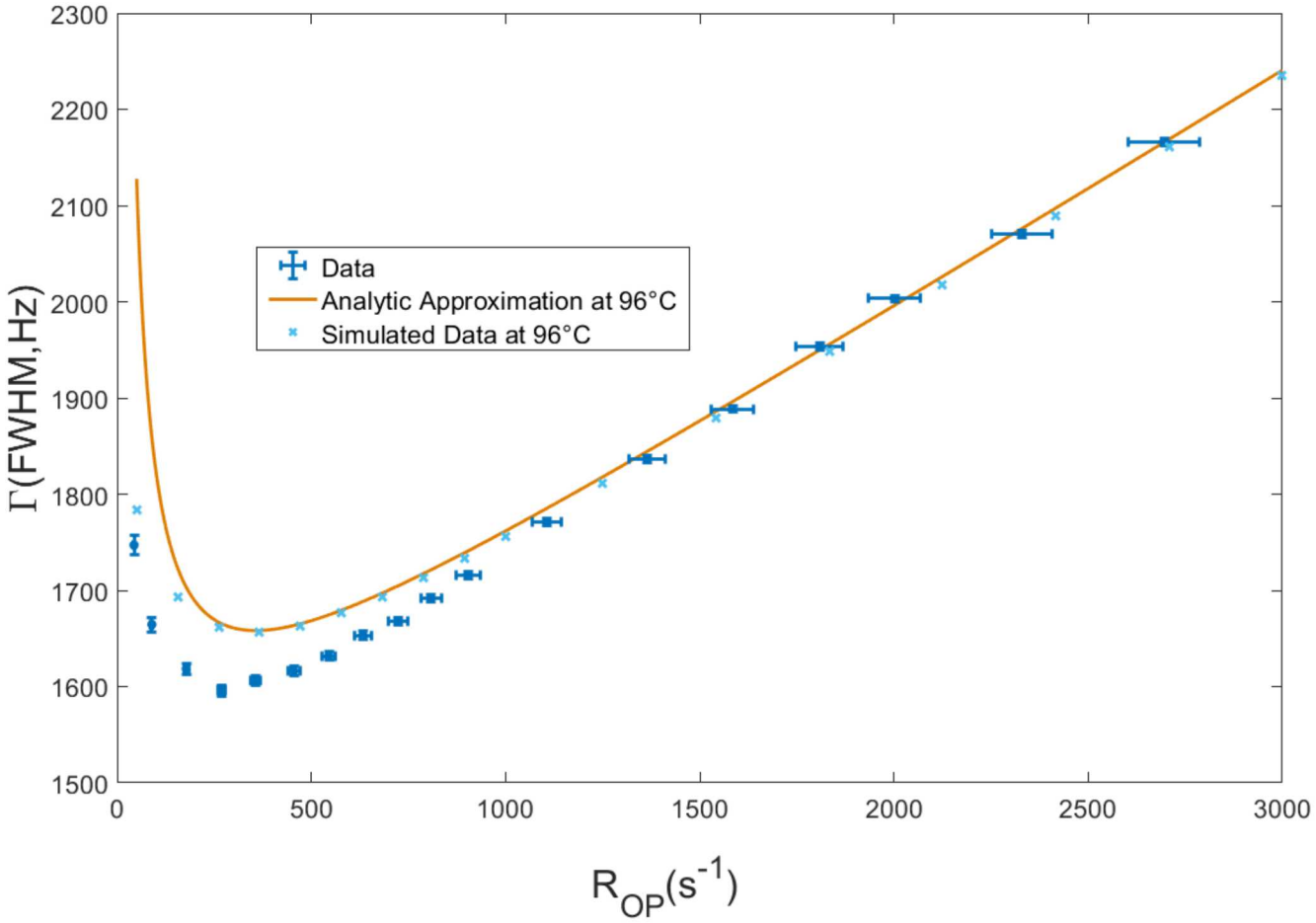

Above: Comparison of data to the analytic approximation $\Gamma \approx \frac{R_{OP}}{4} + \frac{R_{SE}R_{SD}}{5R_{OP}} + \mathrm{b}$ where R_{SE} and R_{SD} were computed for the temperature $T = 96^{\circ}C$ as measured from our thermocouple. The result from a fit based on numerical simulations of the density matrix is also included.

Part 3-II: Experimental Sensitivity

Noise Floor Near 21.5kHz

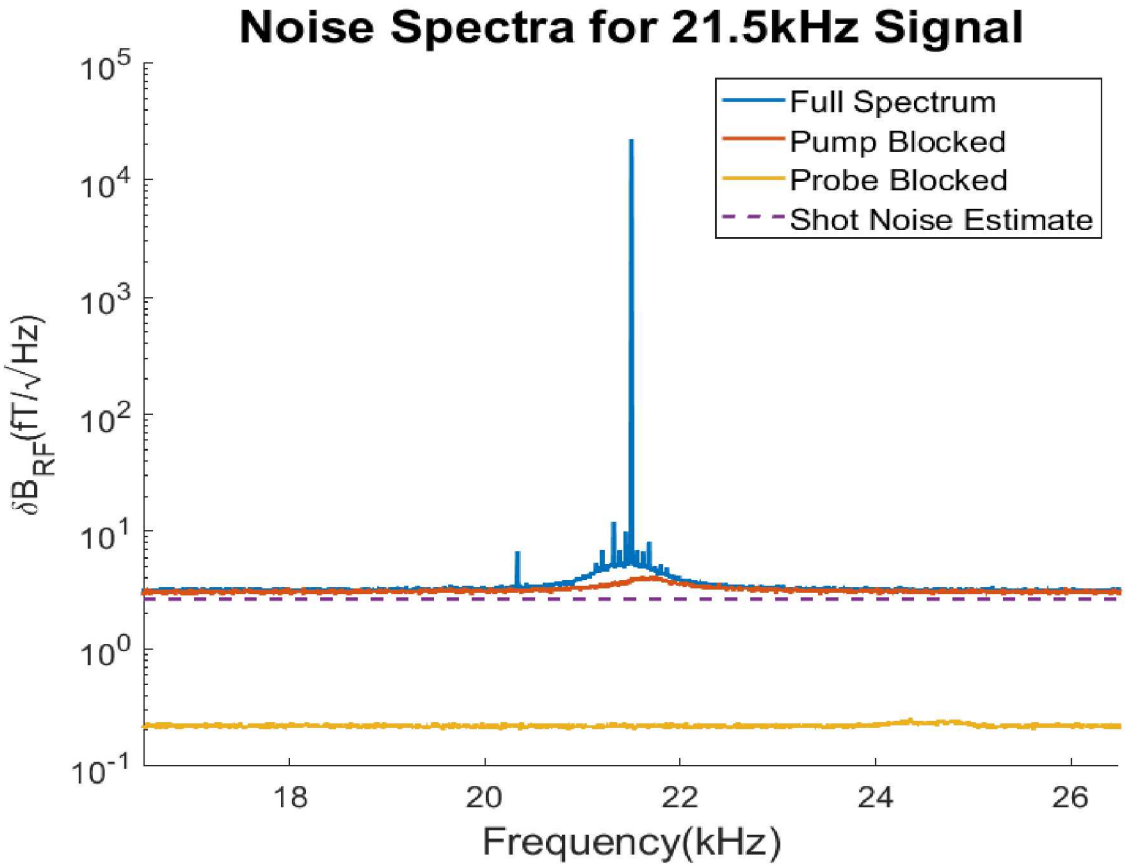

Above: The response of the magnetometer to an input of $B_{RF} = 47\text{pT}$. This is comparable to the result of Savukov et al. who demonstrated a $5\text{fT}/\sqrt{Hz}$ sensitivity in an Rb magnetometer.(11)

Total Noise: Phase and Quadrature Components

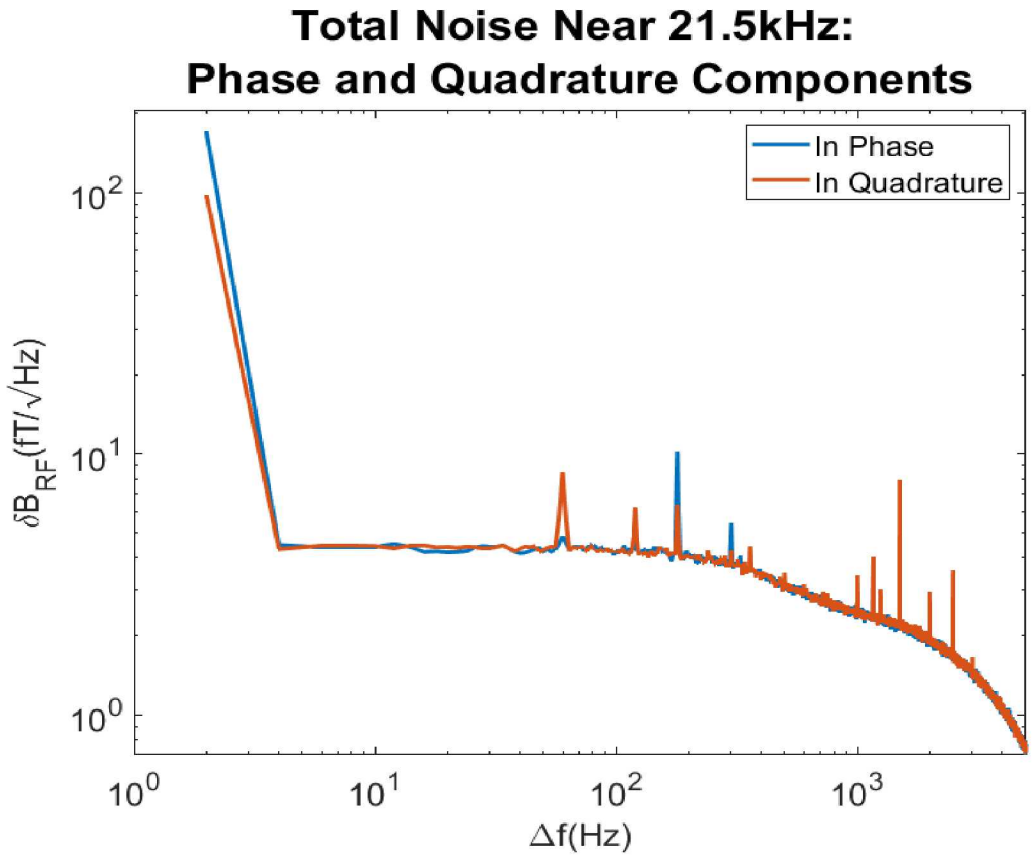

Above: In-phase(I) and in-quadrature(Q) components of the signal found from a lock-in amplifier. Comparability of I and Q shows that there is not significant background DC/low frequency field noise.

Conclusions on Demonstrated Sensitivity

- We have achieved world-class sensitivity in our prototype!
- May be able to do better with slightly higher buffer gas pressure:
  - Analysis of pressure broadening shows we only have $\approx 87Torr$ of N_2. Well resolved hyperfine lines mean we can only pump on $F = 2$ transition.
- We can move on to communications demonstration for real signals!

Part 4: Future Work

Short Term & Medium (By the end of the Year)

1. Test cell with natural abundance of ^{85}Rb and ^{87}Rb & compare to theory
   - Expand simulation framework to support multiple species.
2. Begin work with communications team for demonstration of ability to receive signals of interest.
   - Demo waveform currently being designed.
3. Begin design that does not require μ-metal shields.
   - Requires active feedback on coils to zero out DC and low frequency fields.
4. Begin design of custom fabricated apparatus to house optics in compact package.

Long Term (By the end of the Project, 2022)

1. Complete compact mobile platform.
   - Include active DC/low frequency feedback to zero out fields.
   - Minimize power while maintaining sufficient sensitivity.
2. Create automatic tuning system that tunes RF resonance to the proper place based on user input.
3. Take it outside into an unshielded environment and pick up real signals with it

Part III: Acknowledgements

The RF Magnetometer

- Thanks to Sandia National Labs for providing funding through the laboratory directed research and development (LDRD) program for this work.
- Thanks to Peter Schwindt for giving me the opportunity to work on this project, and his continuing mentorship.
- Thanks to Neil Claussen for his ongoing help with all aspects of the project.

Above: Peter Schwindt

Below: Neil Claussen

References

(1) Bradley et al. "Microwave Cavity Searches for Dark-Matter Axions". Rev. Mod. Phys. **75**, 777(2003).

(2) Chalupczak et al. "Room temperature femtotesla radio-frequency atomic magnetometer". Appl. Phys. Lett. **100**, 242401 (2012)

(3) Garroway et al. "Remote Sensing by Nuclear Quadrupole Resonance". IEEE Trans. Geosci. Remote Sens. **39**,1108(2001)

(4) Gerginov et al. "Prospects for magnetic field communications and location using quantum sensors". Rev. Sci. Inst. **88**, 125005 (2017).

(5) Ledbetter et al. "Detection of radio-frequency magnetic fields using nonlinear magneto-optical rotation". Phys. Rev. A **75**, 023405 (2007)

(6) S.-K Lee et al. "Subfemtotesla radio-frequency atomic magnetometer for detection of nuclear quadrupole resonance". Appl Phys. Lett. **89,** 214106 (2006)

(7) Savukov, Seltzer, and Romalis. Detection of NMR signals with a radio-frequency atomic magnetometer". Jour. Mag. Res. **185-2** (2007).

(8) Savukov et al. "High-sensitivity operation of single-beam optically pumped magnetometer in a kHz frequency range". Meas. Sci. & Tech. (2017)

(9) Savukov et al. "MRI with an atomic magnetometer suitable for practical imaging applications. Jour. Mag. Res. **199-2**. (2009)

(10) Savukov, et al."Tunable Atomic magnetometer for Detection of Radio-Frequency Magnetic Fields". PRL **95**,063004(2005).

(11) Savukov, Karaulanov, and Boshier. "Ultra-sensitive high-density Rb-87 radio-frequency magnetometer". Appl. Phys. Lett. **104**, 023504 (2014)

(12) Seltzer "Developments in Alkali-Metal Atomic Magnetometry". Princeton Ph.D Thesis. (2008)